Enhanced Stability for Propene Epoxidation with H_2 and O_2 over Wormhole-like Hierarchical TS-1 Supported Au Nanocatalyst

Nan Sheng[a], Zhikun Liu[a], Zhaoning Song[a], Dong Lin[a], Xiang Feng[a,c,*], Yibin Liu[a],

Xiaobo Chen[a], De Chen[c], Xinggui Zhou[b], Chaohe Yang[a]

[a] *State Key Laboratory of Heavy Oil Processing, China University of Petroleum, Qingdao 266580,China*

[b] *State Key Laboratory of Chemical Engineering, East China University of Science and Technology, 130 Meilong Road, Shanghai 200237, China*

[c] *Department of Chemical Engineering, Norwegian University of Science and Technology, Trondheim 7491, Norway*

Abstract: Designing highly efficient Au/Ti-containing catalysts for propene epoxidation with H_2 and O_2 harbors tremendous scientific and industrial importance. In this work, novel hydrophobic hierarchical TS-1 (HTS-1) with wormhole-like mesopores (ca. 45 nm) and small crystal size (100 nm) is firstly synthesized by a two-step crystallization method using CTAB as template. Gratifyingly, the Au/HTS-1 catalyst shows simultaneously high PO formation rate of 150 $g_{po}h^{-1}kg_{Cat}^{-1}$ without any promoter additive, PO selectivity of 90 % and impressive stability of 100 h, which are much better than traditional Au/TS-1 catalyst. Furthermore, the intrinsic reason for the enhanced performance is elucidated by multi-techniques such as N_2 physisorption, HRTEM, TGA, FT-IR and ^{29}Si NMR. Interestingly, it is found that the coke in 0.10 wt% Au/HTS-1 catalyst partly reside in mesopores, alleviating the deactivation of micropore blocking. Moreover, the enhanced mass transfer ability and higher hydrophobicity of Au/HTS-1 catalyst also lead to reduced coke weight and absence of aromatic coke.

Keywords: Stability; TS-1; Hydrophobicity; Hierarchical zeolite; Propene epoxidation.

1. Introduction

Propylene oxide (PO), as a fundamental chemical feedstock for the manufacture of polyurethane and polyester resin, is the third largest propene derivative. In comparison to the main traditional processes of chlorohydrination and co-oxidation, the direct propene epoxidation with H_2 and O_2 has many advantages such as environmental friendly, energy saving and simple [1-3]. Haruta and coworkers [4] published their discovery in 1998 that nanoscale gold particles on Ti-containing oxides achieve high selectivity (~95 %) towards gas phase propene epoxidation with H_2 and O_2. Since then, Au/Ti-containing supports (eg., Au/TS-1, Au/uncalcined TS-1, Au/Ti-MCM-41, Au/Ti-TUD, Au/SiO$_2$ and Au/Ti-3D mesoporous titanosilicate) have been extensively studied to improve catalytic performance [5-12]. Delgass et al. reported the highest PO formation rate on Cs promoted Au/TS-1 catalyst, nevertheless, the Au/TS-1 catalysts still suffer from severe deactivation [13].

To date, efforts have been devoted to simultaneously improving the stability and stable activity of Au/TS-1 catalysts [2, 5, 14-15]. It is reported that [16-23] on Au/TS-1 catalyst, the narrow micropore channels of TS-1 (MFI structure of ca. 0.55 nm) limit the diffusion of the PO products, leading to side products and carbonaceous deposits on Au-Ti active sites. Recently, we first reported that constructing hierarchical Au/HTS-1 catalyst could extend the life time of Au/Ti-containing catalyst to 40 h [5]. This shows a new direction to simultaneously enhance the stability and activity, aiming at commercially desirable performance [2]. Along this line, it is highly desirable to design novel hierarchical and hydrophobic TS-1, which can delay the blocking of diffusion path

and facilitate PO desorption [16, 24-26].

Besides the design of novel catalyst, it is of great scientific essential to further investigate on the coke properties such as coke location [27, 28]. Due to the presence of mesopores of hierarchical Au/TS-1 catalyst, the catalyst structure during reaction is more complex. More information on coke properties is thus urgently needed for the design of other efficient Au/Ti-containing catalysts.

In this paper, we propose a novel hierarchical TS-1 (HTS-1) zeolite by two-step crystallization process using cheap cetyltrimethylammonium bromide (i.e., CTAB) as template. Compared with traditional TS-1, the wormhole-like HTS-1 zeolite has the properties of high hydrophobicity and wormhole-like pores, which are beneficial for PO formation. Moreover, the relationship between the physicochemical structure of Au/HTS-1 catalyst and catalytic performance is further elucidated by multi-techniques such as XRD, N_2 physisorption, ^{29}Si NMR, HRTEM, TGA-DTG, FT-IR and UV-vis. The reason for the enhanced performance (e.g., coke location, weight and surface properties of support) is further discussed. This work not only proposes a novel wormhole-like TS-1 support which is effective for propene epoxidation with H_2 and O_2, but also demonstrates new direction of enhancing catalytic performance using hierarchical Au/TS-1 catalyst.

2. Experimental section

2.1 Catalyst preparation

A modified dissolution-recrystallization method [29] was used to prepare HTS-1 according to the following procedure. First, 22.58 g tetraethylorthosilicate (TEOS, 95

wt%) were added dropwise to 27.9 g of tetrapropylammonium hydroxide solution (TPAOH, 25 wt%) under stirring in a Teflon beaker. Afterwards, a required amount of titanium (IV) tetrabutoxide (TBOT, 99 wt%) dissolved in 3.6 g isopropanol (IPA, 99.5 wt%) was added dropwise. The mixture was stirred for 1 h and then heated in a Teflon-lined stainless steel autoclave at 170 ℃ for 24 h under autogenous pressure. The product was collected by filtration, washed with water, dried at room temperature and then calcined for 10 h at 550 ℃. Subsequently, 4 g of the as-obtained TS-1 and 2.8 g cetyltrimethylammonium bromide were added into aqueous ammonium hydroxide (400 mL, 2.5 wt%) solution, and then stirred for 5 h at room temperature. The solution was then transferred to a Teflon-lined stainless steel autoclave and heated to 140 ℃ for 24 h. The product was collected by filtration, washed with deionized water, dried overnight, and then calcined at 550 ℃ for 6 h to remove the surfactant. The as-obtained production was labeled as HTS-1. The synthesizing process of HTS-1 is shown in Fig. 1. In addition, the traditional TS-1 with Si/Ti ratio of 100 was synthesized using hydrothermal method developed by Khomane et al [30].

Au/HTS-1 and Au/TS-1 catalysts were prepared as follows: 0.01 g $HAuCl_4$ and 10ml H_2O were vigorously stirred at 25 ℃ for 30 min. After adjusting the pH of the solution to 7.3~7.6 using 1 M and 0.1 M NaOH solutions, 0.5 g of support was added into the above 0.5 ml solution and then aged at room temperature for hours. Finally, the catalyst was washed twice with deionized water via centrifugation and dried at room temperature overnight.

(Fig. 1 should be inserted here)

2.2 Characterization of the catalysts

The bulk structure of TS-1 and HTS-1 catalysts were carried out with a X'pert PRO MPD diffractometer instrument using Cu-K$_\alpha$ radiation (36 kv, 30 mA). The N$_2$ adsorption-desorption isotherms were measured on a Micromeritics ASAP 2020 instrument. The ultraviolet-visible spectroscopy (UV-vis) spectra of the supports were collected using a PerkinElmer Lambda 35 spectrophotometer, using pure BaSO$_4$ as reference. Fourier transform infrared spectroscopy (FT-IR) spectra of the catalysts were recorded on a Nicolet NEXUS 670 spectrometer using KBr as background. The Au loadings in the catalysts were provided by inductively coupled plasma optical emission spectrometry (ICP-OES) on an Agilent 730 ICP-OES spectrometer. The high resolution transmission electron microscopy (HRTEM) and scanning electron microscopy (SEM) images were taken on a JEOL JSM-2100F microscope and a Hitachi S-4800 field-emission scanning electron microscope, respectively. The weights of carbonaceous deposits were analyzed by thermogravimetric analysis (TGA, PerkinElmer TGA Pyris 1). The TGA analysis was performed by heating dried sample from room temperature to 800 ^{o}C in a flow of N$_2$/O$_2$ = 8:1 at a ramping rate 5 ^{o}C/min. The ^{29}Si solid-state MAS NMR measurements of TS-1 and HTS-1 samples were performed using a Unity/Inova (Varian, 600 MHz) spectrometer operating at the designed frequencies of 119.182 MHz. The ^{29}Si NMR spectra were obtained under the following conditions: 2.0 μs pulse, 7 s relaxation delay, 15 kHZ spinning rate, and 820 acquisitions.

2.3 Catalytic testing

The gas-phase propene epoxidation with H_2 and O_2 was taken in a quartz tubular reactor (i.d., 8 mm) using a feed of C_3H_6, H_2, O_2 and N_2 with the flow rate of 3.5/3.5/3.5/24.5 mL·min^{-1} (a space velocity of 14000 mL h^{-1} g$_{cat}$$^{-1}$). The Au/TS-1 and Au/HTS-1 catalysts (0.15 g) were tested under atmospheric pressure. The reactants and products were analyzed using on-line GC (Agilent 6890). Hydrocarbons, H_2, O_2, N_2, CO_x and H_2O were analyzed in TCD. Oxygenates such as propylene oxide, ethanal, propanal, acetone, acrolein and hydrocarbons were analyzed in FID. Blank tests indicated that no PO was generated in the blank reactor.

Propylene conversion = mol of (C_3-oxygenates + 2/3ethanal + CO_2/3)/mol of propene in the feed.

PO selectivity = mol of PO/mol of (C_3-oxygenates + 2/3ethanal + CO_2/3).

H_2 efficiency = mol of PO/mol of H_2 converted.

3. Results and discussion

3.1. Characterization of hierarchical titanium silicalite-1

Fig. 2a shows the XRD patterns for TS-1, HTS-1 and Au/HTS-1. The MFI structures of the three samples show similar diffraction peaks located at 2θ =7.8°, 8.8°, 23.1°, 23.9° and 24.3°. The lack of the splitting at the peak of ca. 24.3° indicates the formation of the orthorhombic phase. No obvious Au peaks are detected because of low Au loading and uniform Au nanoparticles. Moreover, it is also noted that compared with TS-1, the HTS-

1 and Au/HTS-1 sample also show good crystallinity. This is beneficial to the catalytic performance. In addition, there is broadening of XRD diffraction peaks of HTS-1 and Au/HTS-1, indicating the reduction of crystal size [31]. The N_2 adsorption-desorption isotherms of the TS-1 and HTS-1 samples with the insets of pore-size distributions are shown in Fig. 2b. Firstly, the rapid elevation of the curve at $P/P_0 < 0.02$ for the two samples indicates the existence of micropores. Secondly, the adsorption-desorption curves of HTS-1 sample exhibit typical IUPAC type IV isotherms with a H4 hysteresis loop, which is characteristic of porous materials with narrow slit like wedge-shaped pores. The capillary condensation occurs at P/P_0 ranging from ca. 0.45 to 0.95 is observed, which is due to multilayer adsorption of nitrogen molecules inside mesoporous [32]. The corresponding pore-size distribution indicates that the HTS-1 sample has not only micropores with diameters of ca. 0.55 nm, but also mesoporous larger than 10 nm. The peak of mesopores locates at ca. 45 nm. These constitute the hierarchically porous structure of HTS-1. In contrast, no mesopores exist in TS-1 support. The apparent BET surface area and pore volume of TS-1 and HTS-1 are listed in Table 1. The BET surface areas of TS-1 and HTS-1 are 437 and 418 m^2g^{-1}, respectively. The slightly reduced BET surface area of HTS-1 is ascribed to the less micropores. However, HTS-1 support owns larger total and mesopore volume 0.38 and 0.19 cm^3g^{-1}, respectively, because of the hierarchical structure.

(Fig. 2 should be inserted here)

(Table 1 should be inserted here)

It is known that only isolated Ti (IV) species in the TS-1 framework is essential for selective propene epoxidation with H_2 and O_2. This can be analyzed by DRUV-vis. Fig. 3a shows the DRUV-vis spectra of TS-1 and HTS-1. The absorption peaks at around 220 nm indicate the incorporation of the titanium into MFI framework for both TS-1 and HTS-1 samples, confirming the presence of isolated Ti (IV) species in the MFI framework. No significant extra framework titanium is found in any of the TS-1 samples, as evidenced by the absence of absorption peaks attributed to anatase TiO_2 in the 330 nm region [32, 33]. Moreover, the results of UV-vis characterization are in good agreement with the FT-IR spectra in Fig. 3b. For the TS-1 and HTS-1 samples, the band at 960 cm^{-1} is often considered as a proof of Ti substitution into the framework in the form of Ti-O-Si. The adsorption bands at 800 and 1100 cm^{-1} are attributed to the symmetrical and antisymmetrical stretching vibration of $[SiO_4]$ units, respectively. The bands at 550 and 1230 cm^{-1} are the vibration of double five-membered ring and asymmetrical stretching vibration of MFI framework structure, respectively. This is in accordance with the reported FT-IR spectra of typical TS-1 [16, 34, 35]. The UV-vis and FT-IR show that both of the samples have only isolated Ti^{4+} species.

(Fig. 3 should be inserted here)

Fig. 4 shows the typical SEM and TEM images of TS-1 and HTS-1 samples. The shapes of both samples are regular and berry-like. Compared with TS-1 which shows a larger particle size of ca. 500 nm, the HTS-1 sample exhibits a significantly reduced particle size of ca. 100 nm. This could be ascribed to the synthetic mechanism of HTS-1 sample prepared by an alkaline dissolution-reassembly process in the presence of a

surfactant. In the first step, small TS-1 crystals as seeds serve as the TS-1 nuclei, which contribute to crystal growth by attachment. At the early stage of the synthesis process, large number of crystals nucleus are formed and the crystals slowly grow after nucleation. This should be the main reason for smaller particle size of HTS-1. Moreover, TS-1 seeds are dissolved in an aqueous solution of ammonium hydroxide and CTAB, and the reassembly is performed in an autoclave under hydrothermal conditions. Based on the synthetic mechanism reported by Ivanova et al [36, 37], the alkaline dissolution breaks Si-O-Si bonds inside the zeolite, which leads to the formation of intra-particle voids and mesopores. With the surfactant CTAB, the surfactant can protect the zeolite from random base leaching, resulting in the formation of extra large mesopores. Moreover, the surfactant CTAB serves as the template for the condensation of dissolved Si and Ti species during the hydrothermal reassembly. Fig. 4 (c, d) show the typical TEM images of the two samples. It is confirmed that intra-particle voids and mesopores are found in the HTS-1 sample. The mean mesopore size agrees well with the pore size estimated from the BJH pore size distribution (Fig. 2b).

(Fig. 4 should be inserted here)

3.2 Catalytic performance of Au/HTS-1 and Au/TS-1 catalysts

Fig. 5 shows the HRTEM images of the Au/HTS-1 and Au/TS-1 catalysts. More than 150 nanoparticles are measured to determine Au average particle size so as to increase accuracy. It is obvious that the average Au nanoparticle size of the Au/HTS-1 (3.0 nm) is almost the same to that of Au/TS-1 catalyst (3.1 nm).

(Fig. 5 should be inserted here)

Fig. 6 presents the catalytic performance of the Au/HTS-1 and the traditional Au/TS-1 catalysts for propene epoxidation with H_2 and O_2. To make a fair comparison, the Au loadings of the two catalysts are similar (ca. 0.10 wt %). It is obvious that the traditional Au/TS-1 catalyst gave higher initial PO formation rate (ca. 160 $g_{po}h^{-1}kg_{Cat}^{-1}$). However, the traditional Au/TS-1 catalyst has severe deactivation as PO formation rate sharply decreases from 160 to 115 $g_{po}h^{-1}kg_{Cat}^{-1}$. This is mainly because part of the tiny Au clusters incorporated into the microporous channels of traditional TS-1 are highly active for PO production but not easily accessible to reactants due to micropore blocking by carbonaceous deposits [18, 23, 38]. In contrast, the Au/HTS-1 catalysts showed more stable performance for 100 h with PO formation rate of 150 $g_{po}h^{-1}kg_{Cat}^{-1}$. Increasing Au loading from 0.10 to 0.15 wt% leads to the increase of PO formation rate from 150 to 280 $g_{po}h^{-1}kg_{Cat}^{-1}$. Nevertheless, it is noted that as the Au loading increases to 0.15 wt%, there is reduction of micropore volume and thus deactivation for the Au/HTS-1 catalyst caused by coke formation. The higher initial activity may be because more Au clusters residing into some of micropores could achieve a higher initial PO formation rate when Au loading is higher. However, higher PO formation rate leads to more coke, and more catalytic sites are easily blocked by coke in limited space of the micropores. Furthermore, as the Fig. 7a shows, there is a little decrease of selectivity from 83 to 78%. It was reported that larger Au particle has much worse PO selectivity. This indicates sintering of the Au nanoparticles also happens for 0.15 wt% Au/HTS-1 catalyst. Therefore, it is concluded that the deactivation is mainly caused by coke formation, and the sintering of the Au

nanoparticles also happens when the Au loading is high.

(Fig. 6 should be inserted here)

(Fig. 7 should be inserted here)

The detailed selectivities of the catalysts are presented in Fig. 7a. The PO selectivity of the traditional Au/TS-1 catalyst is ca. 89 %. It is surprising that all Au/HTS-1 catalysts show PO selectivity larger than 90 %, comparable to and even a little higher that of the traditional Au/TS-1 catalyst. Furthermore, the detailed products selectivities of Au/HTS-1 and Au/TS-1 are showed in Fig. 7b. Propanal and carbon dioxide are the main side products for Au/HTS-1 and Au/TS-1 catalysts formed by ring-opening reaction and deep oxidation[21]. It is noteworthy that the H_2 efficiency (29 %) of Au/HTS-1 catalyst is higher than that of Au/TS-1 catalyst (22 %). The H_2 efficiency for this reaction is closely relevant to the formation and decomposition of H_2O_2. Since the H_2O_2 is easily decomposed at reaction temperature of 200 ^oC, the improved mass transfer ability of the Au/HTS-1 catalyst could accelerate transfer process of H_2O_2 from Au sites to Ti_4^+ sites, increasing the H_2 efficiency.

3.3 The underlying reasons for the superior performance of Au/HTS-1 catalyst

To elucidate the underlying reasons for the distinctive performance of the Au/HTS-1 catalyst, the properties of the catalysts were further analyzed after reaction. Fig. 8a presents the TGA results of the Au/HTS-1 and Au/TS-1 catalysts at reaction time of 200 ^oC after 25 h. The total coke weight of the Au/TS-1 catalyst (i.e., 4.9 wt%) is much larger than that of the Au/HTS-1(i.e., 2.7 wt%), indicating that coke is easier to form on the

Au/TS-1 catalyst and the ability of coke formation on the Au/HTS-1 catalyst is effectively inhibited. The micropore and mesopore volumes of the fresh Au/HTS-1 catalyst and the same Au/HTS-1 catalyst at reaction temperature of 200 $^{\circ}$C after reaction of 100 h are presented in Table 2. Interestingly, the results show that both the micropore and mesopore volume of the Au/HTS-1 after reaction comparatively decreases. This suggests that the formed coke also partly reside in mesopores with less hindrance. Therefore, mesopores are the key to enhance the mass transfer ability to get long catalyst lifetime, and micropores are the key to make sure the high PO formation rate. This effectively alleviates the micropore blocking by carbonaceous deposits and avoids the deactivation for Au/HTS-1 catalyst.

Table 2 should be inserted here.

The DTG curves of the Au/TS-1 and Au/HTS-1 catalysts are presented in Fig. 8b. For Au/HTS-1 catalyst, two DTG peaks are present between 340 and 550 $^{\circ}$C, which stand for the different kinds of carbonaceous deposits. It is noted that the higher decomposition temperature represents the heavier carbonaceous deposits. In contrast, the refractory carbonaceous deposits, corresponding to the DTG peak at 650 $^{\circ}$C, exist on the Au/TS-1 catalyst. Therefore, the heavier carbonaceous deposits is easier to be formed on the Au/TS-1 catalyst.

(Fig. 8 should be inserted here)

The properties of the carbonaceous deposits are also investigated by FT-IR, which are showed in Fig. 8. For the Au/TS-1 catalyst, three bands are observed at 1350-1470, 1600-1650 and 1700-1750 cm^{-1}, which are attributed to branched alkanes, polyalkenes

and refractory aromatic species, respectively. However, the band at 1700-1750 cm^{-1}, which stands for refractory aromatic species, could not be observed for the Au/HTS-1 catalyst [38]. It can be concluded that better transfer ability endowed by the hierarchical pore structure of the Au/HTS-1 catalyst could not only reduce coke weight but also lead to the absence of refractory aromatic species in Au/HTS-1 catalyst.

(Fig. 9 should be inserted here)

(Fig. 10 should be inserted here)

Apart from the mass transfer ability, another key parameter affecting deactivation of the catalyst and coke weight is hydrophobicity. The ^{29}Si MAS NMR spectra of the Au/TS-1 and Au/HTS-1 catalysts are used to detect the hydrophobicity (Fig. 10). The low intensity of the Q3 peak at -105 ppm in the ^{29}Si spectra is attributed to the $(SiO)_3SiOH$ species and the high intensity of the Q4 peak at -115 ppm in the ^{29}Si spectra stands for the $Si(SiO)_4$ species [7, 39, 40]. The relative Q3/Q4 ratio of the Au/HTS-1 is about 4%, which indicates the number of silanol groups per Si site in the Au/HTS-1 catalyst. In contrast, the relative Q3/Q4 ratio of the Au/TS-1 is about 9.5 %, much larger than that of Au/HTS-1 catalyst, demonstrating the TS-1 support has more hydroxyl groups than HTS-1 support [41]. The less surface hydroxyl groups indicates the improved hydrophobicity of Au/HTS-1 catalyst, which favors desorption of PO and suppresses side reactions on catalyst surface [20]. Furthermore, the improved hydrophobicity of Au/HTS-1 catalyst explains why less refractory carbonaceous deposits are generated in the Au/HTS-1 catalyst.

The reaction mechanism of propene epoxidation with H_2 and O_2 is that Au sites are

mainly responsible for formation of H_2O_2, and Ti sites are responsible for formation of Ti-OOH intermediate for subsequent propene epoxidation [18, 42]. If the PO product could not desorb from the Ti sites in time or be absorbed in other active sites, the absorbed PO could open its ring to form the branched alkanes, which are further converted into ployalkenes and subsequent aromatic species [43]. Therefore, the origin of high stability of the Au/HTS-1 catalyst can be attributed to three factors. First, the Au/HTS-1 catalyst has improved the mass transfer ability due to small particle size, which hampers the formation and evolution of refractory carbonaceous deposits. Second, the wormhole-like pores of this Au/HTS-1 catalyst could provide more room for carbonaceous deposits, making micropore blocking less possible. In addition, the higher hydrophobicity of the Au/HTS-1 catalyst could also suppress ring-opening reaction of PO production on catalyst surface, improving the stability and the PO stable activity of Au/HTS-1 catalyst.

Table 3 shows the catalytic performance of the reported stable Au/HTS-1 and Au/Ti-containing catalysts taken from the literature [2, 5, 14-15]. All the reported catalysts are quite promising for propene epoxidation. In comparison, the Au/HTS-1 catalyst shows high stability and stable activity. Furthermore, the Au/HTS-1 catalyst achieves a higher activity than the Au/MTS-1 catalyst possibly because of its better crystallinity. This work shows the reported highest stability and also fascinating PO formation rate. The work is also of great referential importance to the design of efficient Au/Ti-containing catalysts for other reactions (e.g., propane selective oxidation [44]).

4. Conclusions

In conclusion, hierarchical TS-1 (HTS-1) with intracrystalline pore size of ca. 45 nm and small crystal size (100 nm) is first synthesized by a two-step crystallization method using CTAB as template. The Au/HTS-1 catalyst shows fantastic PO formation rate (ca. 150 $g_{po}h^{-1}kg_{Cat}^{-1}$) and stability (ca. 100 h), which are higher than traditional Au/TS-1 catalyst. The intrinsic reasons for the improved performance of the Au/HTS-1 catalyst are enhanced mass transfer ability and better hydrophobicity, resulting in less coke weight and absence of aromatic coke. Furthermore, the formed coke partly reside in mesopores which has less hindrance, alleviating the deactivation. This work proposes a novel wormhole-like TS-1 support by the two-step crystallization method and also demonstrates the strategy of enhancing catalytic performance by designing hierarchical Au/TS-1 catalyst. The strategy and insights about mesopores-metal system may shed a new light on the design of long-lifetime and high-selectivity zeolite supported metallic catalysts.

References

1. G. Wu, Y. Wang, L. Wang, W. Feng, H. Shi, Y. Lin, T. Zhang, X. Jin, S. Wang, and X. Wu, Epoxidation of propylene with H_2O_2 catalyzed by supported TS-1 catalyst in a fixed-bed reactor: experiments and kinetics. Chem. Eng. J. 215-216 (2013) 306-314.

2. J. Huang, T. Takei, and T. Akita, Gold clusters supported on alkaline treated TS-1 for highly efficient propene epoxidation with O_2 and H_2. Appl. Catal. B 95 (2010) 430-438.

3. T. Hayashi, K. Tanaka, and M. Haruta, Selective vapor-phase epoxidation of propylene over Au/TiO$_2$ catalysts in the presence of oxygen and hydrogen. J. Catal. 178 (1998) 566-575.

4. M. Haruta, B.S. Uphade, S. Tsubota, and A. Miyamoto, Selective oxidation of propylene over gold deposited on titanium-based oxides. Res. Chem. Intermed. 24 (1998) 329-336.

5. X. Feng, N. Sheng, Y. Liu, X. Chen, D. Chen, C. Yang, and X. Zhou, Simultaneously enhanced stability and selectivity for propene epoxidation with H_2 and O_2 on Au catalysts supported on nano-crystalline mesoporous TS-1. ACS Catal. 7 (2017) 2668-2675.

6. W.S. Lee, L.C. Lai, M.C. Akatay, E.A. Stach, F.H. Ribeiro, and W.N. Delgass, Probing the gold active sites in Au/TS-1 for gas-phase epoxidation of propylene in the presence of hydrogen and oxygen. J. Catal. 296 (2012) 31-42.

7. X. Feng, D. Chen, and X.G. Zhou, Thermal stability of TPA template and size-dependent selectivity of uncalcined TS-1 supported Au catalyst for propene epoxidation with H_2 and O_2. RSC Adv. 6 (2016) 44050-44056.

8. A.K. Sinha, S. Seelan, T. Akita, S. Tsubota, and M. Haruta, Vapor phase propylene epoxidation over Au/Ti-MCM-41 catalysts prepared by different Ti incorporation modes. Appl. Catal. A 240 (2003) 243-252.

9. A.K. Sinha, S. Seelan, S. Tsubota, and M. Haruta, A three-dimensional mesoporous titanosilicate support for gold nanoparticles: vapor-phase epoxidation of propene with high conversion. Angew. Chem. Int. Ed. 43 (2004) 1546-1548.

10. J. Lu, X. Zhang, J.J. Bravo-Suárez, K.K. Bando, T. Fujitani, and S.T. Oyama, Direct propylene epoxidation over barium-promoted Au/Ti-TUD catalysts with H_2 and O_2: effect of Au particle size. J. Catal. 250 (2007) 350-359.

11. G. Mul, A. Zwijnenburg, B.V.D. Linden, M. Makkee, and J.A. Moulijn, Stability and selectivity of Au/TiO_2 and Au/TiO_2/SiO_2 catalysts in propene epoxidation: an in situ FT-IR study. J. Catal. 201 (2001) 128-137.

12. H. Peng, L. Xu, L. Zhang, K. Zhang, Y. Liu, H. Wu, and P. Wu, Synthesis of core-shell structured TS-1@mesocarbon materials and their applications as a tandem catalyst. J. Mater. Chem. 22 (2012) 14219-14227.

13. W.S. Lee, M.C. Akatay, E.A. Stach, F.H. Ribeiro, and W.N. Delgass, Enhanced reaction rate for gas-phase epoxidation of propylene using H_2 and O_2 by Cs promotion of Au/TS-1. J. Catal. 308 (2013) 98-113.

14. B.S. Uphade, M. Okumura, S. Tsubota, and M. Haruta, Effect of physical mixing of CsCl with Au/Ti-MCM-41 on the gas-phase epoxidation of propene using H_2 and O_2:: drastic

depression of H_2 consumption. Appl. Catal. A 190 (2000) 43-50.

15. J Huang, E. Lima, T. Akita, C Qi, M. Haruta, Propene epoxidation with O_2 and H_2: identification of the most active gold clusters. J. Catal. 278 (2011) 8-15.

16. X. Feng, X. Duan, H. Cheng, G. Qian, D. Chen, W. Yuan, and X. Zhou, Au/TS-1 catalyst prepared by deposition-precipitation method for propene epoxidation with H_2/O_2: insights into the effects of slurry aging time and Si/Ti molar ratio. J. Catal. 325 (2015) 128-135.

17. Z. Li, J. Zhang, W. Ma, Confirmation of gold active sites on titanium-silicalite-1-supported nano-gold catalysts for gas-phase epoxidation of propylene. J. Phys. Chem. B, 121 (2017) 25215-25222.

18. X. Lu, G. Zhao, Y. Lu, Propylene epoxidation with O_2 and H_2: a high-performance Au/TS-1 catalyst prepared via a deposition-precipitation method using urea. Catal. Sci. Technol. 3 (2013) 2906-2909.

19. B. Chowdhury, J.J. Bravo-Suárez, M. Daté, S. Tsubota, and M. Haruta, Trimethylamine as a gas-phase promoter: highly efficient epoxidation of propylene over supported gold catalysts. Angew. Chem. Int. Ed. 118 (2006) 426-429.

20. X. Feng, Y. Liu, Y. Li, C. Yang, Z. Zhang, X. Duan, X. Zhou, and D. Chen, Au/TS‑1 catalyst for propene epoxidation with H_2/O_2: a novel strategy to enhance stability by tuning charging sequence. AIChE J. 62 (2016) 3963-3972.

21. X. Feng, X. Duan, J. Yang, G. Qian, X. Zhou, D. Chen, and W. Yuan, Au/uncalcined TS-1 catalysts for direct propene epoxidation with H_2 and O_2: effects of Si/Ti molar ratio and Au loading. Chem. Eng. J. 278 (2015) 234-239.

22. X. Feng, X. Duan, Q. Gang, X. Zhou, D. Chen, and W. Yuan, Au nanoparticles deposited on the external surfaces of TS-1: enhanced stability and activity for direct propylene epoxidation with H_2 and O_2. Appl. Catal. B 150 (2014) 396-401.

23. X. Feng, X. Duan, G. Qian, X. Zhou, D. Chen, and W. Yuan, Insights into size-dependent activity and active sites of Au nanoparticles supported on TS-1 for propene epoxidation with H_2 and O_2. J. Catal. 317 (2014) 99-104.

24. R. Gounder and M.E. Davis, Beyond shape selective catalysis with zeolites: hydrophobic void spaces in zeolites enable catalysis in liquid water. AIChE J. 59 (2013) 3349-3358.

25. W. Song, Z. Yi, G. Xiong, X. Zhang, F. Jin, L. Liu, and X. Wang, Transformation of SiO_2 in titanium silicalite-1/SiO_2 extrudates during tetrapropylammonium hydroxide treatment and improvement of catalytic properties for propylene epoxidation. Chem. Eng. J. 253 (2014) 464-471.

26. G.J. Soler-Illia, C. Sanchez, B. Lebeau, and J. Patarin, Chemical strategies to design textured materials: from microporous and mesoporous oxides to nanonetworks and hierarchical structures. Chem. Rev. 102 (2002) 4093-4138.

27. L.D. Rollmann and D.E. Walsh, Shape selectivity and carbon formation in zeolites. J. Catal. 56 (1979) 139-140.

28. A. Ruiz, B.V.D. Linden, M. Makkee, and G. Mul, Acrylate and propoxy-groups: contributors to deactivation of Au/TiO_2 in the epoxidation of propene. J. Catal. 266 (2009) 286-290.

29. J. Mielby, J.O. Abildstrøm, F. Wang, T. Kasama, C. Weidenthaler, and S. Kegnaes, Oxidation of bioethanol using zeolite-encapsulated gold nanoparticles. Angew. Chem. Int. Ed. 126 (2014) 12721-12724.

30. G. Zhan, M. Du, D. Sun, J. Huang, X. Yang, Y. Ma, A.R. Ibrahim, and Q. Li, Vapor-phase propylene epoxidation with H_2/O_2 over bioreduction Au/TS-1 catalysts: synthesis, characterization, and optimization. Ind. Eng. Chem. Res. 50 (2011) 9019-9026.

31. A. Thangaraj, R. Kumar, S.P. Mirajkar, and P. Ratnasamy, Catalytic properties of crystalline titanium silicalites I. synthesis and characterization of titanium-rich zeolites with MFI structure. J. Catal. 130 (1991) 1-8.

32. Z. Wang, L. Xu, J.G. Jiang, Y. Liu, M. He, and P. Wu, One-pot synthesis of catalytically active and mechanically robust mesoporous TS-1 microspheres with the aid of triblock copolymer. Micropor. Mesopor. Mater. 156 (2012) 106-114.

33. D.P. Serrano, R. Sanz, P. Pizarro, I. Moreno, and S. Medina, Hierarchical TS-1 zeolite as an efficient catalyst for oxidative desulphurization of hydrocarbon fractions. Appl. Catal. B 146 (2014) 35-42.

34. T. Armaroli, F. Milella, B. Notari, R.J. Willey, and G. Busca, A spectroscopic study of amorphous and crystalline Ti-containing silicas and their surface acidity. Top. Catal. 15 (2001) 63-71.

35. G.N. Vayssilov, Structural and physicochemical features of titanium silicalites. Catal. Rev. 39 (1997) 209-251.

36. I.I. Ivanova and E.E. Knyazeva, Micro-mesoporous materials obtained by zeolite recrystallization: synthesis, characterization and catalytic applications. Chem. Soc. Rev. 42 (2013) 3671-88.

37. I.I. Ivanova, I.A. Kasyanov, A.A. Maerle, and V.I. Zaikovskii, Mechanistic study of zeolites recrystallization into micro-mesoporous materials. Micropor. Mesopor. Mater. 189 (2014) 163-172.

38. L.D. Rollmann, Systematics of shape selectivity in common zeolites. J. Catal. 47 (1977) 113-121.

39. H. Wang and T.J. Pinnavaia, MFI zeolite with small and uniform intracrystal mesopores. Angew. Chem. Int. Ed. 118 (2010) 7765-7768.

40. S. Du, X. Chen, Q. Sun, N. Wang, M. Jia, V. Valtchev, and J. Yu, A non-chemically selective top-down approach towards the preparation of hierarchical TS-1 zeolites with improved oxidative desulfurization catalytic performance. Chem. Commun. 52 (2016) 3580-3583.

41. K. Na, C. Jo, J. Kim, W.S. Ahn, and R. Ryoo, MFI titanosilicate nanosheets with single-unit-cell thickness as an oxidation catalyst using peroxides. ACS Catal. 1 (2011) 901-907.

42. K. Zhou, J. Jia, C. Li, F. Wei, A low content Au-based catalyst for hydrochlorination of C_2H_2 and its industrial scale-up for future PVC processes. Green Chem. 17 (2015) 356-364.

43. A. Zwijnenburg, M. Makkee, and J.A. Moulijn, Increasing the low propene epoxidation product yield of gold/titania-based catalysts. Appl. Catal. A 270 (2004) 49-56.

44. J.J. Bravo-Suárez, K.K. Bando, T. Fujitani, Mechanistic study of propane selective oxidation with H_2 and O_2 on Au/TS-1. J. Catal. 257 (2008) 32-42.

Table captions:

Table 1 Structural properties of TS-1 and HTS-1 supports.

Table 2 Pore volumes of 0.10 wt% Au/HTS-1 catalysts before and after reaction.

Table 3 Catalytic properties of stable Au/Ti-containing catalysts for propene epoxidation with H_2 and O_2.

Table 1 Structural properties of TS-1 and HTS-1 supports.

Supports	S_{BET} (m^{2}g^{-1})	V_{tot}^{a} (cm^{3}g^{-1})	V_{micro}^{a} (cm^{3}g^{-1})	V_{meso}^{a} (cm^{3}g^{-1})
TS-1	437	0.23	0.16	0.07
HTS-1	418	0.38	0.17	0.19

^{a} V_{tot}, V_{micro}, and V_{meso} represent the total, microporous, and mesoporous volume, respectively.

Table 2 Pore volumes of 0.10 wt% Au/HTS-1 catalysts before and after reaction.

Catalyst	$V_{micro}{}^{a}(cm^3g^{-1})$	$V_{meso}(cm^3g^{-1})$
Au/HTS-1(fresh)	0.167	0.196
Au/HTS-1(100 h)	0.148	0.173

[a] The micropore volume is calculated by the t-plot method.

Table 3 Catalytic properties of stable Au/Ti-containing catalysts for propene epoxidation with

H_2 and O_2.

samples	Au loading (wt%)	PO selectivity (%)	Stability (h)	Reaction temperature (^{o}C)	Space velocity ($mLg_{Cat}^{-1}h^{-1}$)	PO formation rate ($g_{po}h^{-1}kg_{Cat}^{-1}$)	reference
Au/HTS-1[a]	0.10	90.0	100	200	14000	150	This work
Au/MTS-1	0.13	95.2	40	200	14000	142	5
Au/TS-1-B	0.12	83.0	30	200	14000	125	14
Au/TS-1-SA	0.15	90.0	40	200	14000	153	20
Au/TS-1-SG	0.10	85.0	16	200	8000	119	2
Au/TS-1-IL	1.0	65.0	48	300	4000	75	30

[a] Reaction condition: 0.15 g of catalyst; feed gas, $C_3H_6/H_2/O_2/N_2$ = 3.5/3.5/3.5/24.5 $mLmin^{-1}$, space velocity = 14000 $mLg_{Cat}^{-1}h^{-1}$; feed pressure = 1 atm; reaction temperature = 473 K.
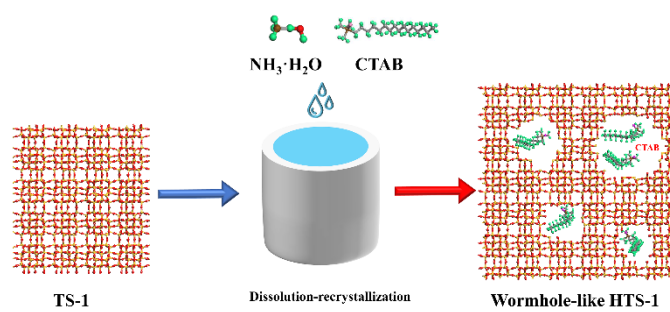
Figure captions:

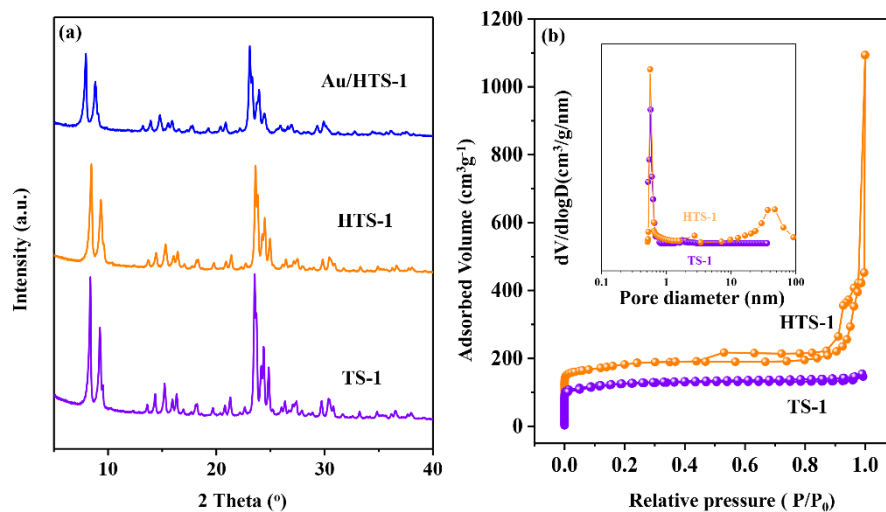**Fig. 1.** Synthesis of the HTS-1 zeolite.

Fig. 2. (a) XRD spectra of HTS-1 and TS-1, (b) N_2 adsorption-desorption isotherms of HTS-1 and TS-1. The inset in Fig. 1b shows the pore size distributions of HTS-1 and TS-1.
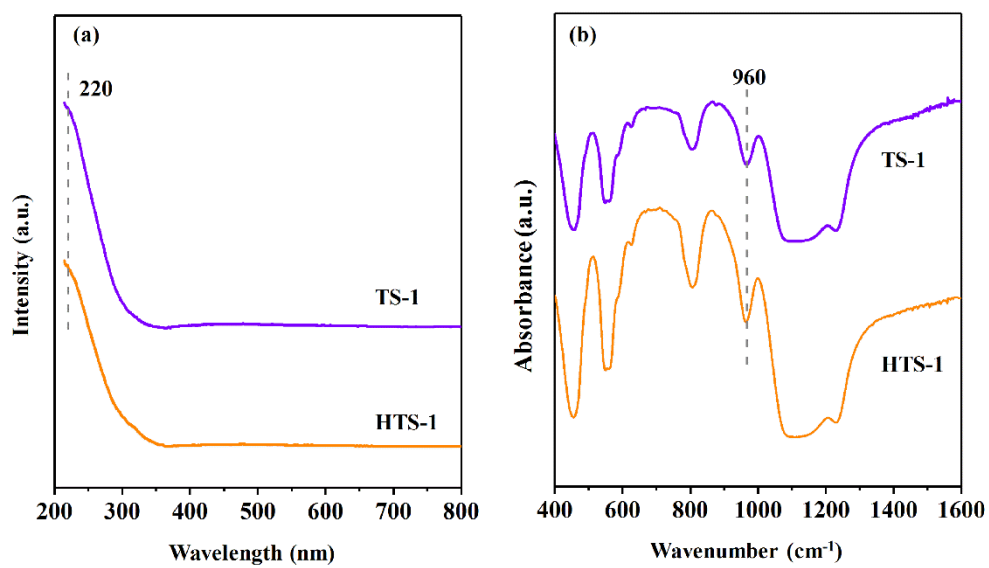
Fig. 3. (a) UV-vis spectra (b) FT-IR spectra of TS-1 and HTS-1 samples.
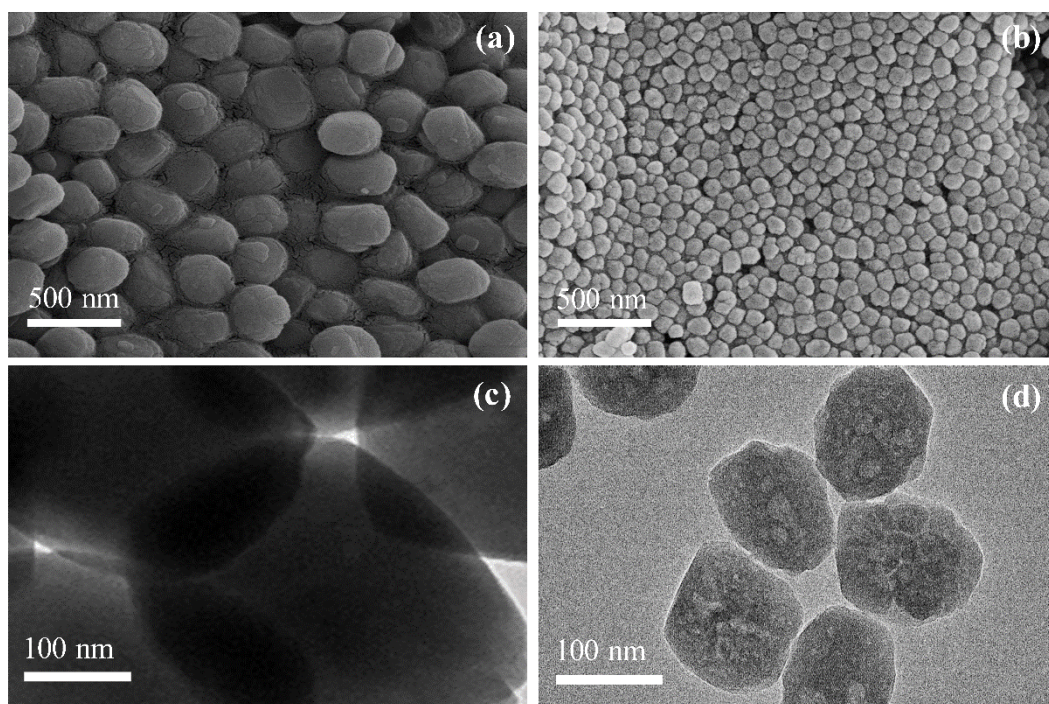
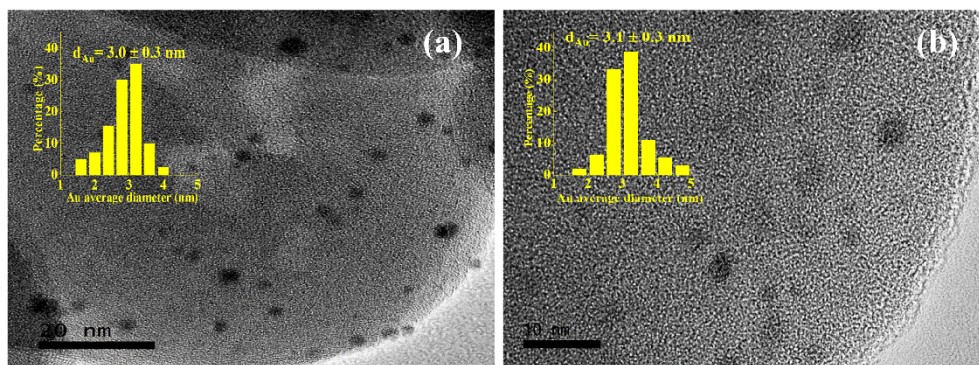**Fig. 4.** Representative SEM and TEM images of (a,c) TS-1 and (b,d) HTS-1.

Fig. 5. HRTEM images of (a) Au/HTS-1 and (b) Au/TS-1 catalysts. The insets show the Au size distributions of the catalysts, and the scale bars represent 20 nm and 10 nm, respectively.
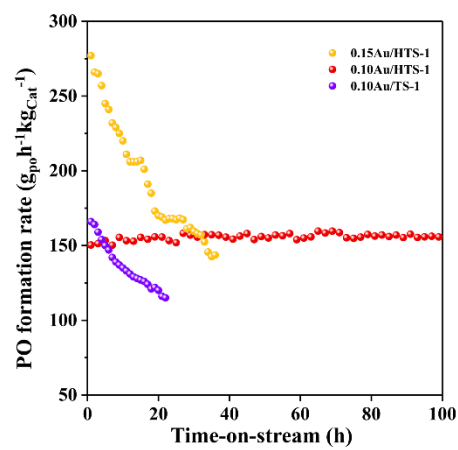
Fig. 6. PO formation rate of Au/HTS-1 and Au/HTS-1 catalyst at different time-on-stream.

Fig. 7. PO selectivities (a) of 0.10 and 0.15 wt% Au/HTS-1 and 0.10 wt% Au/TS-1; Detailed products distributions (b) of Au/HTS-1 and Au/TS-1 with the same Au loadings of 0.10 wt%.

Fig. 8. TGA (a) and DTG (b) curves of Au/HTS-1 and Au/TS-1 catalysts at 200 ^{o}C for 25 h.

Fig. 9. FT-IR spectra of Au/TS-1 and Au/HTS-1 catalysts at 200 ^{o}C for 25 h.

Fig. 10. ^{29}Si MAS NMR spectra of TS-1 (a) and HTS-1 (b) supports.

Fig. 1. Synthesis of the HTS-1 zeolite.

Fig. 2. (a) XRD spectra of HTS-1 and TS-1, (b) N_2 adsorption-desorption isotherms of HTS-1 and TS-1. The inset in Fig. 2b shows the pore size distributions of HTS-1 and TS-1.

Fig. 3. (a) UV-vis spectra (b) FT-IR spectra of TS-1 and HTS-1 samples.

Fig. 4. Representative SEM and TEM images of (a,c) TS-1 and (b,d) HTS-1.

Fig. 5. HRTEM images of (a) Au/HTS-1 and (b) Au/TS-1 catalysts. The insets show the Au size distributions of the catalysts, and the scale bars represent 20 nm and 10 nm, respectively.

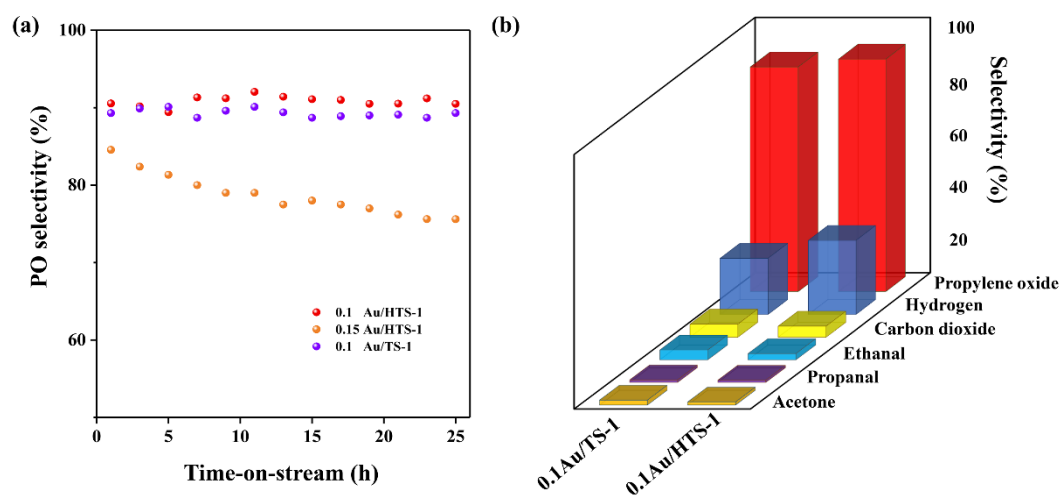**Fig. 6.** PO formation rate of Au/HTS-1 and Au/HTS-1 catalyst at different time-on-stream.

Fig. 7. PO selectivities (a) of 0.10 and 0.15 wt% Au/HTS-1 and 0.10 wt% Au/TS-1; Detailed

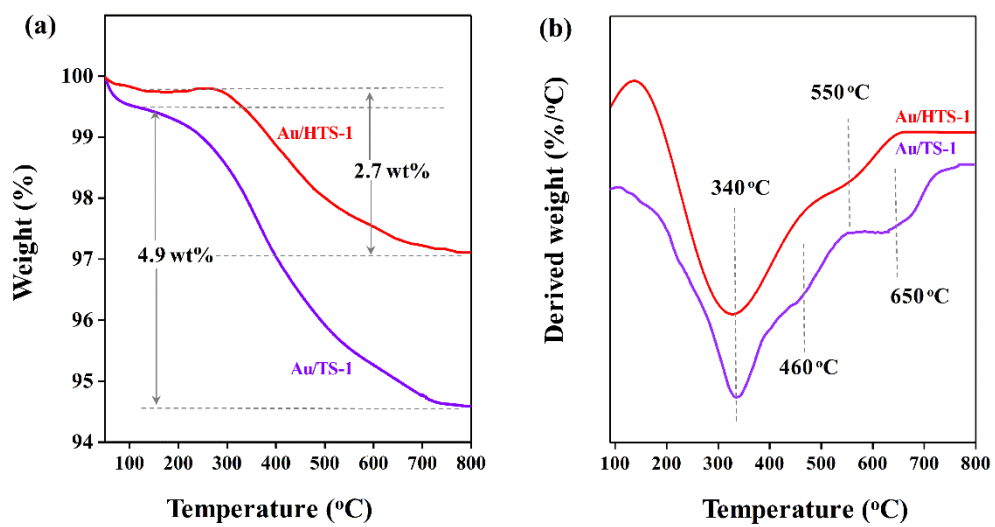products distributions (b) of Au/HTS-1 and Au/TS-1 with the same Au loadings of 0.10 wt%.

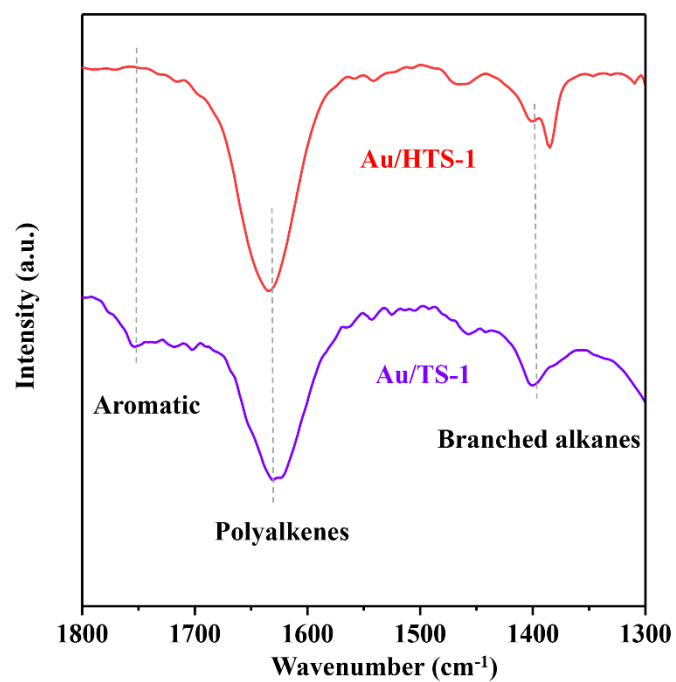**Fig. 8.** TGA (a) and DTG (b) curves of Au/HTS-1 and Au/TS-1 catalysts at 200 °C for 25 h.

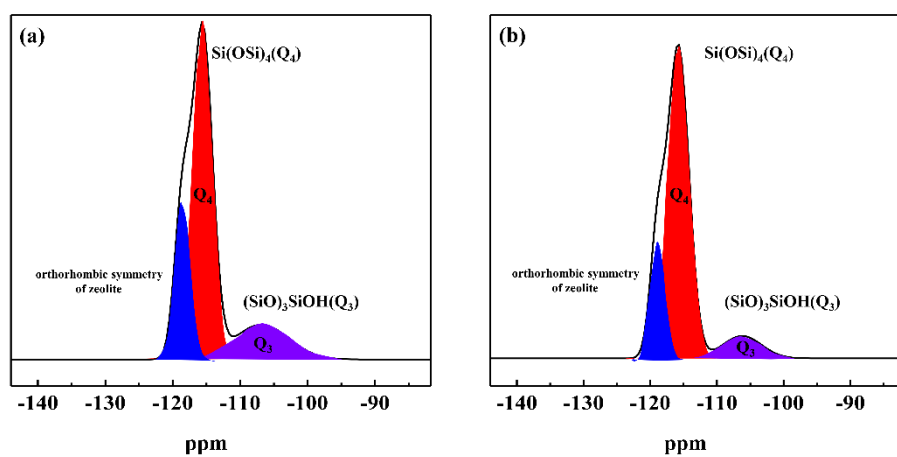**Fig. 9.** FT-IR spectra of Au/TS-1 and Au/HTS-1 catalysts at 200 ºC for 25 h.

Fig. 10. ^{29}Si MAS NMR spectra of TS-1 (a) and HTS-1 (b) supports.